

Received October 25, 2021, accepted November 23, 2021, date of publication November 30, 2021, date of current version December 10, 2021.

Digital Object Identifier 10.1109/ACCESS.2021.3131344

A Contactless Planar Inductive Sensor for Absolute Angular Displacement Measurement

WENZHENG GAO¹, HONG SHI¹, AND QIFU TANG², (Member, IEEE)

¹Department of Control Equipment, Lianyungang JARI Electronics Company Ltd., Lianyungang, Jiangsu 222061, China

²Engineering Research Center of Mechanical Testing Technology and Equipment, Ministry of Education, Chongqing University of Technology, Chongqing 400054, China

Corresponding author: Qifu Tang (sealy1@126.com)

ABSTRACT This paper proposes a new planar inductive sensor with printed circuit boards (PCB) based stator and rotor, which can perform more precision measurement than traditional inductive angular displacement sensors. The sensor uses PCB technique to realize accurately configured planar coils. The stator consists of a ferromagnetic base plate and a PCB with three groups of circular excitation coils and two groups of sine shape pickup coils working as two sense channels. The rotor consists of a ferromagnetic base plate and a PCB with two circles of copper pieces. Copper pieces on the rotor PCB produce eddy current in the time-varying magnetic field and alter the outputs of two sense channels of pickup coils cyclically with the rotor's rotation. Two sense channels can make incremental angle measurement individually and work together to make absolute angle measurement. A prototype with 63 and 64 period sense channels was designed and developed for experiments, and test results show that it was finally examined with short-period error of 14.7'' and full range error of 20.6''. The possessed characteristics of inductive principle, absolute measuring and good accuracy make this type of sensor is very suitable for high precision, reliable measurement in harsh environments.

INDEX TERMS Contactless, inductive sensor, absolute angular displacement, eddy current, PCB.

I. INTRODUCTION

Planar displacement sensors based on PCB technique have been developed rapidly in recent years, such as capacitive and inductive sensors, as they are very suitable in many industrial or outdoor environments where most optical based sensors cannot work because they are generally delicate facing dust, moisture, water, lubricant, strong vibration, etc.. Planar capacitive sensors use two PCBs to fabricate stator and rotor electrodes. Planar inductive sensors use one PCB to fabricate primary and secondary coils of the stator and use another PCB or a metallic plate to fabricate the rotor. Netzer position sensors are PCB capacitive displacement sensors [1], which have similar working principle with the sensor proposed in [2]. The capacitance between stator and rotor electrodes varies with the rotor's rotation, and the angular displacement is derived based on two sense signals (sine and cosine signals) of capacitance variations. As we know, the outputs of capacitive based sensors are sensitive to such foreign matters as moisture, water, lubricant, though their applications are not as limited as

optical based sensors in harsh environments. Zettlex IncOder encoders are PCB inductive displacement sensors [3], which have similar working principle with the sensor proposed in [4], [5]. Primary coils on the stator produce electromagnetic field which is received by the coils on the rotor. The coils on the rotor produce another secondary electromagnetic field to act on secondary coils on the stator. With the rotor's rotation, the output signals of the secondary coils vary as sine and cosine patterns. As reported in [3] and [5], there is some improvement space in the measurement accuracy of IncOder encoders compared with capacitive based displacement sensors of equivalent sizes. Posic encoders are also PCB inductive displacement sensors [6], which have similar working principle with the sensor proposed in [7]. The coupling of primary and secondary coils on the sensor head is altered by the copper pieces on the rotor PCB and the output signals of the secondary coils also vary as sine and cosine patterns. Posic or like displacement sensors have very small size, but the measurement accuracy is not as good as Netzer or Zettlex like PCB based sensors.

Besides, there are other researches on the PCB based displacement sensors. [8] proposed an inductive angular

The associate editor coordinating the review of this manuscript and approving it for publication was Abhishek K. Jha .

displacement sensor whose stator coils are fabricated with a PCB. Its rotor is a ferromagnetic plate with planar teeth. The rotor teeth alter the coupling of primary and secondary coils on the stator PCB to realize angle measurement. However, this sensor requires a precision machined ferromagnetic rotor to achieve high precision measurement as well as the sensor presented in [9]. [10] proposed a structure of an inductive absolute angular position sensor. The stator coil consists of a primary coil and two secondary coils laid on a PCB. The rotor is a circular metallic plate with a sector aperture, altering the induced voltage in the secondary coils. This kind of sensor has simple structure, but it has difficulty in realizing precision angle measurement. [11] proposed a linear displacement sensor with a stator PCB and a ferromagnetic U-shape core. The stator has a capacitive sense channel and an inductive sense channel. The core alters the capacitance between the electrodes in the capacitive sense channel and the coils' inductance in the inductive sense channel simultaneously. The displacement is derived by use both of the signals from two sense channels. The accuracy of this sensor is not high and it still has drawbacks of capacitive based sensor due to its capacitive sense channel. Another linear displacement with similar components as [11] is reported in [12], differently it employs an E-shape ferromagnetic core to move and alter the inductances of two coils on a couple of PCBs to measure displacement. The sensor requires a couple of stator PCBs with fine assembling. This requirement may impede its applications. A linear displacement sensor using core-less planar coils on two PCBs is presented in [13]. The sensor consists of two planar stationary coils on one PCB and a moving coil on the other PCB. Displacement is computed by measuring the mutual inductance between the stationary coils and the moving coil. This kind of sensor has to use wires feeding the moving coil, resulting in that it cannot work in the occasions of high movement and reliability.

This paper presents a new planar PCB-type displacement sensor based on eddy current effect that can measure absolute angular displacement. This sensor aims to achieve high accuracy by use of its fine designed coil configuration and software-tuned electrical parameters, besides high reliability owing to contactless structure, inductive based principle, wireless rotor, and low cost owing to simple configuration, easy manufacturing and assembling. Compared with traditional inductive displacement sensors, such as linear variable differential transformers (LVDT), rotary variable differential transformers (RVDT), inductosyns [14], [15] resolvers [16]–[19] and other wire-wound based sensors [20]–[22], this sensor is low-cost and easy to manufacture. Compared with optical and capacitive based angular sensors, this sensor is robust in harsh environments, though its accuracy is not as good as them. Compared with the inductive based PCB-type angular sensors, such as ones introduced above, this sensor can provide measurement with small original error. Following section I, section II introduces the basic structure of the sensor and measurement principles. Section III introduces a prototype of the sensor and

corresponding test platform. Section IV introduces the experiment and results of the sensor prototype. At last, conclusions are summarized.

II. STRUCTURE AND WORKING PRINCIPLE

A. BASIC STRUCTURE OF THE SENSOR

Fig. 1 illustrates the basic structure of the proposed sensor. The stator consists of a ferromagnetic base plate and a PCB with three groups of circular coils and two groups of sine shape coils. Circular coils are the excitation coils to generate magnetic field, while sine shape coils are the pickup coils to output induced voltage in relation to the absolute angle to be measured. Outer and inner groups of excitation coils have same winding direction, while middle group of excitation coils has different winding direction from outer and inner ones. All excitation coils are connected in series. Inner sine shape coils work as one sense channel, and outer ones work as the other sense channel. Every channel of sine shape coils consists of four portions, as shown in Fig. 1(b), where coil $\sin 1+$, $\sin 2+$, $\cos 1+$ and $\cos 2+$ are clockwise, while coil $\sin 1-$, $\sin 2-$, $\cos 1-$ and $\cos 2-$ are counterclockwise. Coil $\sin 1+$ and $\sin 1-$, $\cos 1+$ and $\cos 1-$, $\sin 2+$ and $\sin 2-$, $\cos 2+$ and $\cos 2-$ are connected in series respectively to output two couples of quadrature signals. Two sense channels have different periods of sine shape coils to realize absolute displacement measurement. In the design of the proposed sensor, outer sine shape coils have one more period than inner ones. Every sense channel can measure incremental displacement only. Two sense channels need cooperation to perform absolute displacement measurement. The rotor consists of a ferromagnetic base plate and a PCB with two circles of copper pieces. Copper pieces on the rotor PCB alter the couplings between the excitation coils and pickup coils cyclically with the rotor's rotation due to the eddy current production on them. The eddy current can generate additional magnetic field, as a result, the magnetic density covered by the copper pieces is different from other areas. The magnetic field between the stator and rotor has similar distribution as shown in Fig. 2 of [8]. When the rotor's rotation happens, the magnetic flux received by the pickup coils has cyclical variation which makes the pickup coils output varying voltage.

B. MEASUREMENT PRINCIPLE

When they are supplied with an alternate current signal of $U(t) = U_m \sin(\omega t)$, a time-varying magnetic field is generated in two circular areas between two adjacent circles of excitation coils. Given that inner sense channel of sine shape pickup coils have N periods and outer sense channel has $N + 1$ periods. Inner pickup coils output the signals as expressed by (1) and (2), outer pickup coils output the signals as expressed by (3) and (4).

$$e_{\sin 1}(t, \theta) = k_1 \sin(N\theta) \cdot \cos(\omega t) \quad (1)$$

$$e_{\cos 1}(t, \theta) = k_1 \cos(N\theta) \cdot \cos(\omega t) \quad (2)$$

$$e_{\sin 2}(t, \theta) = k_2 \sin[(N + 1)\theta] \cdot \cos(\omega t) \quad (3)$$

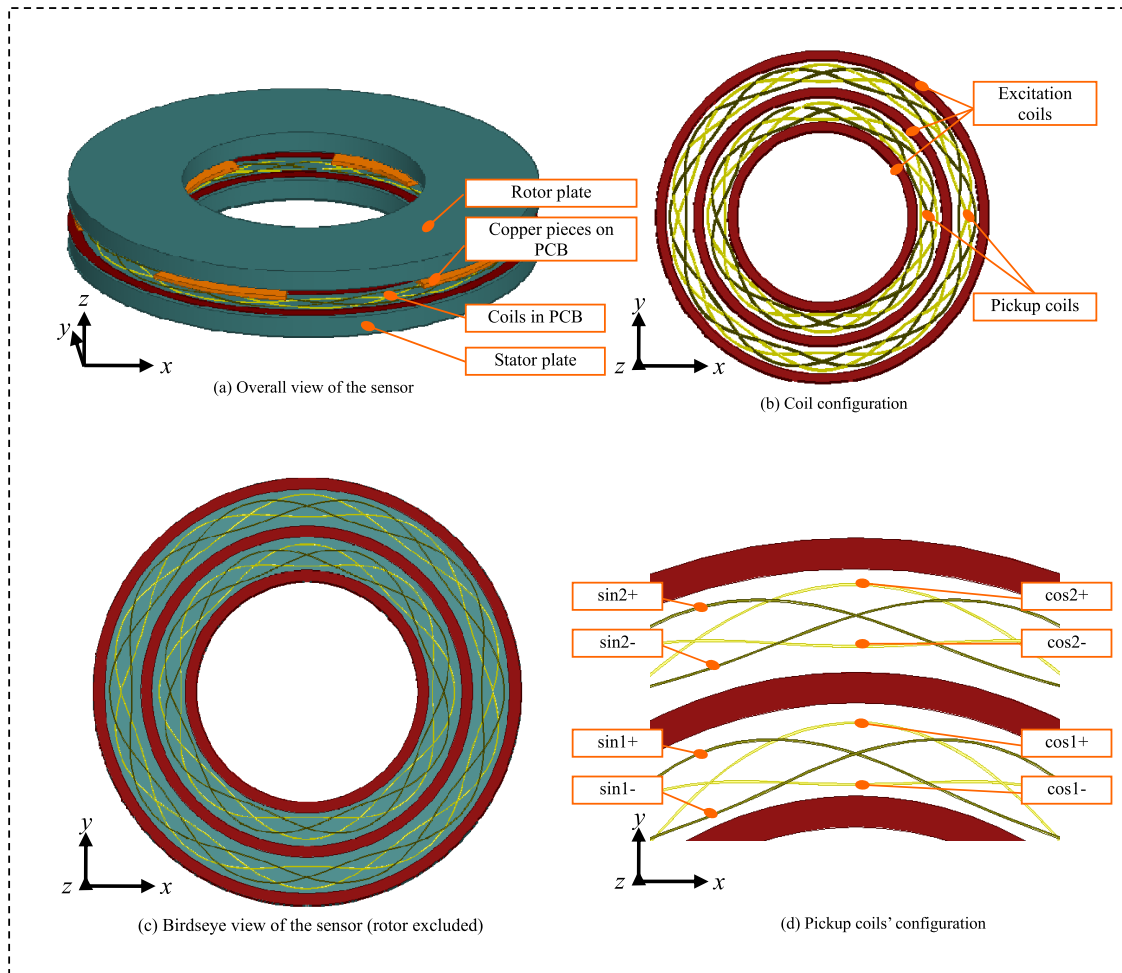


FIGURE 1. Basic structure diagram of the proposed sensor.

$$e_{\cos 2}(t, \theta) = k_2 \cos[(N + 1)\theta] \cdot \cos(\omega t) \quad (4)$$

where k_1 and k_2 are the amplitudes of the signals, θ is the absolute angle to be measured.

Fig. 2 shows the main circuit scheme employed by the proposed sensor. The scheme is designed based on a FPGA. To drive the excitation coils, the FPGA generates a square wave to control a couple of MOSFETs (N-channel + P-channel) first. Then the output of the MOSFET couple is trimmed to a sine signal as $U(t) = U_m \sin(\omega t)$ by a LC low-pass filter (LPF) and a direct current (DC) isolation capacitor. The pickup coils are connected to the mixers containing some switches controlled by a square wave of the same frequency with excitation signal. The signals of (1) to (4) are transformed to ones as (5) to (8) by the mixers. After the processing of the LPFs and amplifiers, high frequency components of signal (5) to (8) are removed. The residual signals can be expressed as (9) to (12), which are low frequency signals related to angular displacement.

$$e_{\sin 1_mix}(t, \theta) = 0.5k_1 \sin(N\theta) \cdot [1 + \cos(2\omega t)] \quad (5)$$

$$e_{\cos 1_mix}(t, \theta) = 0.5k_1 \cos(N\theta) \cdot [1 + \cos(2\omega t)] \quad (6)$$

$$e_{\sin 2_mix}(t, \theta) = 0.5k_2 \sin[(N + 1)\theta] \cdot [1 + \cos(2\omega t)] \quad (7)$$

$$e_{\cos 2_mix}(t, \theta) = 0.5k_2 \cos[(N + 1)\theta] \cdot [1 + \cos(2\omega t)] \quad (8)$$

The analog signal (9) to (12) are converted to digital data by the analog to digital converters (ADCs) and input into the FPGA. Two angle values can be obtained individually using an arctangent operation from digital data of signal (9) and (10), of signal (11) and (12). If we use θ_1 and θ_2 to represent those two angles, then they can be computed using (13) and (14) in an incremental manner, or using (15) and (16) in an absolute manner.

$$e'_{\sin 1}(t, \theta) = k'_1 \sin(N\theta) \quad (9)$$

$$e'_{\cos 1}(t, \theta) = k'_1 \cos(N\theta) \quad (10)$$

$$e'_{\sin 2}(t, \theta) = k'_2 \sin[(N + 1)\theta] \quad (11)$$

$$e'_{\cos 2}(t, \theta) = k'_2 \cos[(N + 1)\theta] \quad (12)$$

$$\theta = 2\pi i_1 / N + \theta_1 / N \quad (13)$$

$$\theta = 2\pi i_2 / (N + 1) + \theta_2 / (N + 1) \quad (14)$$

$$\begin{cases} i_{SN} = \text{RDDN}[(\theta_2 - \theta_1) \cdot (N + 1) / 2\pi] & (\theta_2 \geq \theta_1) \\ i_{SN} = \text{RDDN}[(\theta_2 + 2\pi - \theta_1) \cdot (N + 1) / 2\pi] & (\theta_2 < \theta_1) \end{cases} \quad (15)$$

$$\theta = 2\pi i_{SN} / (N + 1) + \theta_2 / (N + 1) \quad (16)$$

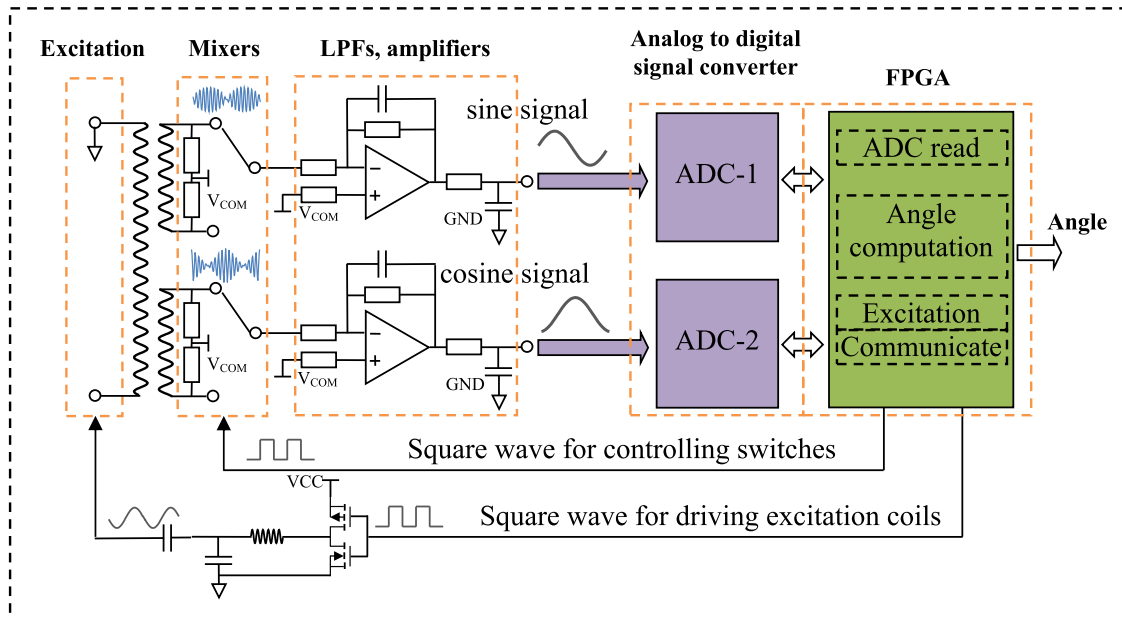


FIGURE 2. Diagram of the main circuit scheme employed by the proposed sensor.

where $k'1$ and $k'2$ are the amplitudes of the signals before ADCs, i_1 and i_2 are the periods that the output signals of inner and outer sense channels vary with the rotor's rotation, RDDN is an operator of rounding down operation, i_{SN} is an integer that represents which region the rotor stops in if we divide the absolute displacement range 0 to 2π into $N + 1$ regions.

If two m -bit ADCs are used to convert the sine and cosine signals, and outer sense channel defines the final angle, the sensor outputs an angle with resolution of $360^\circ / ((N + 1) \cdot 2^m)$. Given that the sensor outputs ideal sine and cosine signals, and ADCs have no conversion error, in theory the measurement accuracy can achieve as good as $360^\circ / ((N + 1) \cdot 2^m)$. However, any stage of the sensor's manufacture or signal processing may introduce error, such as 1) coil layout deviation, 2) not well-distributed magnetic field, 3) not well-assembled PCBs with base plates, 4) stator or rotor eccentricity, 5) non-uniform gap between stator and rotor, 6) demodulation error of sine and cosine signals, 7) ADCs' conversion error, 8) time-varying electronic interference.

III. SENSOR PROTOTYPE AND TEST PLATFORM

A prototype was designed and developed to verify the feasibility of the proposed sensor. Figure 3 shows the layouts of the prototype's stator PCB and rotor PCB. Inner sense channel of the stator PCB was designed with 63 period pickup coils, while outer sense channel was designed with 64 period pickup coils. Correspondingly, the rotor PCB was designed with 63 copper pieces of inner circle and 64 copper pieces of outer circle. Fig. 4 shows the picture of the prototype and its test platform. The prototype's rotor is connected coaxially with a high precision optical encoder (an angle encoder of DR. JOHANNES HEIDENHAIN GmbH with up to $1''$ measurement accuracy outputting 3600000 pulses per

revolution, whose product model is RON886) which serves as a reference. The prototype and the optical encoder are driven to rotate by a rotary table in the test platform. In the conduction of testing the prototype, the position data of the prototype and the optical encoder are synchronously acquired by the test circuit and then transmitted to a computer via a RS232 port.

IV. EXPERIMENT AND RESULTS

A. PRIMARY TEST

The prototype works with a frequency of 125kHz due to that 125kHz is the resonant frequency of the drive circuit for excitation coils and thus makes the coils generate strong magnetic field. Too small or big gap between the stator and rotor can make pickup coils output distorted or too weak signals which may cause big measurement error, as a result, the prototype's working gap was tuned and selected 1mm as the optimal size according to the signal amplitude of the pickup coils and corresponding measurement error. The short-period (a period of inner sense channel: $0^\circ \sim 360^\circ / 63$, a period of outer sense channel: $0^\circ \sim 360^\circ / 64$) errors and full range ($0^\circ \sim 360^\circ$) errors of inner and outer sense channels were examined respectively. The prototype and the optical encoder are driven to rotate by the rotary table with a speed of 0.1rpm. Their position data were sampled and transmitted synchronously to a computer with a period of 2.5ms (this sample period is limited by the RS232 port used in the circuit). The measurement errors were computed by making subtraction of the position data obtained from the prototype and the optical encoder. Fig. 5 to 8 show the error curves in the primary test. 100 points were extracted in a short period and 350 points were extracted in the full range to show the curves clearly. Inner sense channel has the errors of

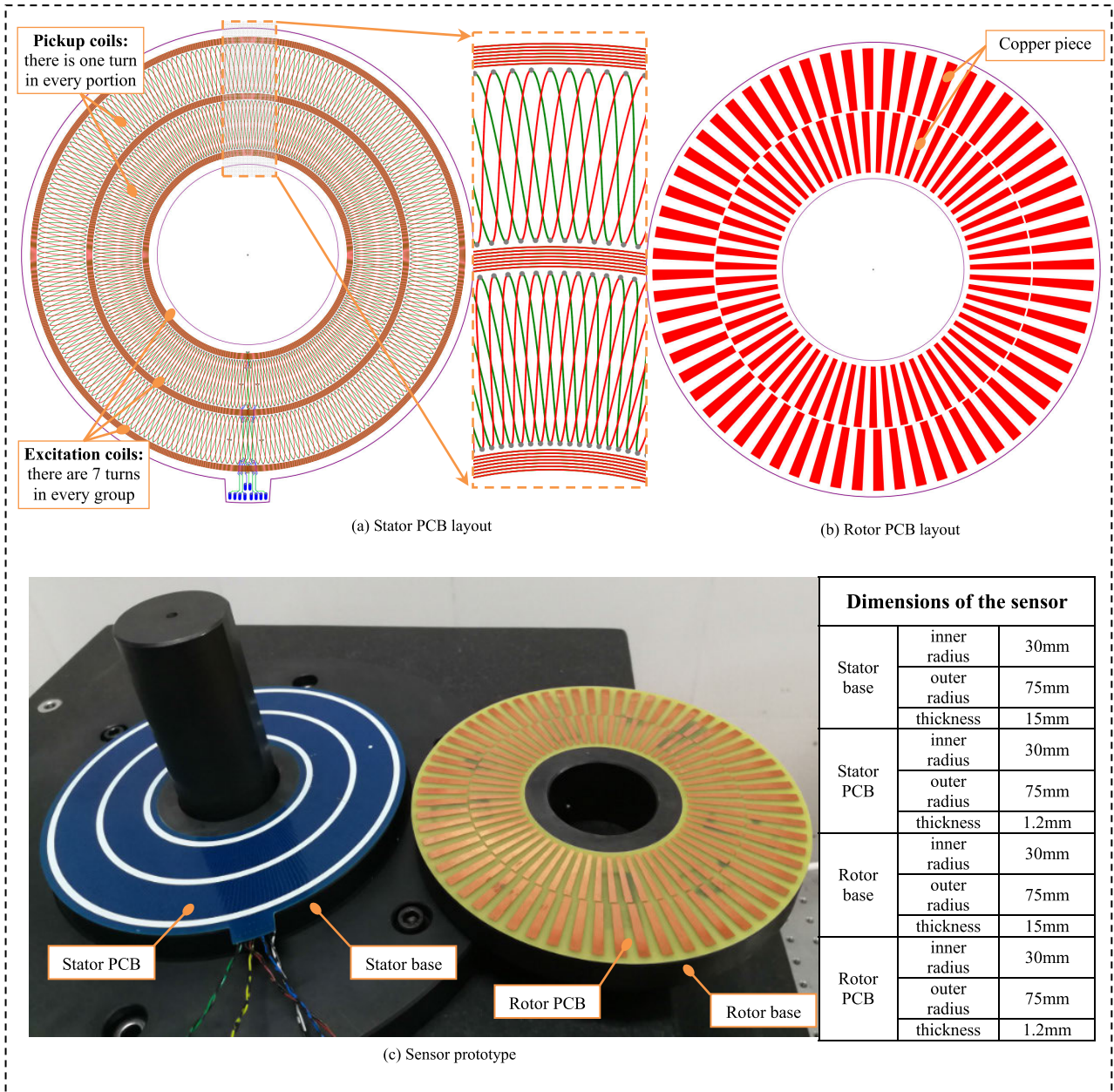


FIGURE 3. Layouts of the stator and rotor PCB and the prototype for experiments.

$-70.9'' \sim 16.3''$ in the range of $0^\circ \sim 5.7^\circ$ ($5.7^\circ \approx 360^\circ/63$),
 $-92.9'' \sim 17.6''$ in the range of $0^\circ \sim 360^\circ$,
 while outer sense channel has the errors of
 $-2.5'' \sim 54.2''$ in the range of $0^\circ \sim 5.625^\circ$ ($5.625^\circ \approx 360^\circ/64$),
 $-4.7'' \sim 60.7''$ in the range of $0^\circ \sim 360^\circ$.

It can be observed from Fig. 5 and 7 that the short-period errors have a significant first-order component.

B. ANALYSIS OF FIRST-ORDER ERROR

In theory, the output signals of pickup coils are zero when there is no rotor above the stator, because the symmetrical

configuration of pickup coils makes the magnetic field received by clockwise and counterclockwise coils cancelled out. However actually, we cannot implement all fabrication stages of the prototype such as PCB layouts, assembling, wire-connecting ideally. As a result, the clockwise and counterclockwise pickup coils are not able to cancel out the received magnetic field with the rotor's absence. In this condition, there is an electromotive force (EMF) which is irrelevant with the rotor's rotation in the regular operation of the prototype. We take the inner sense channel for example to analyze the influence of this EMF. Equation (1) and (2) should be rewritten as (17) and (18) where k_{11} and k_{12} are

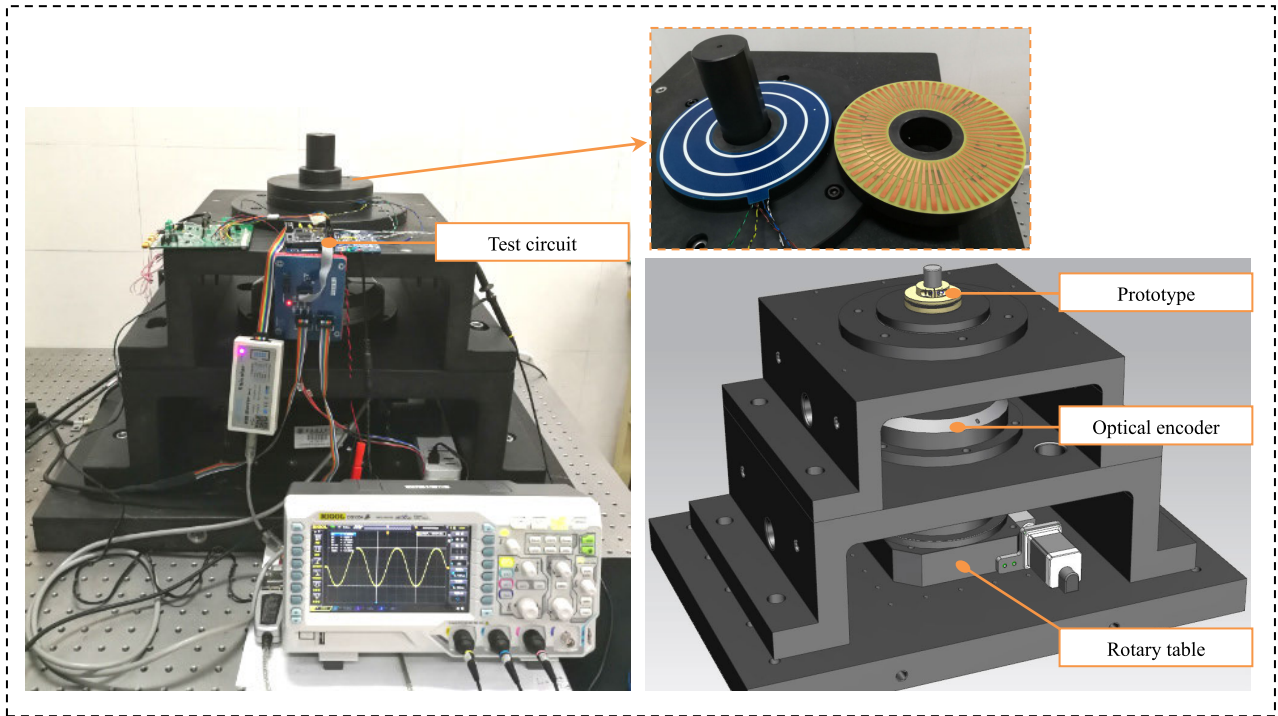


FIGURE 4. Picture of the test platform for examining the prototype.

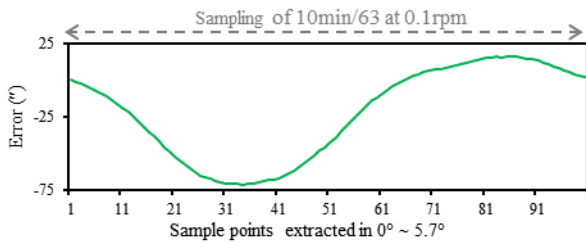


FIGURE 5. Short-period error of inner sense channel in primary test.

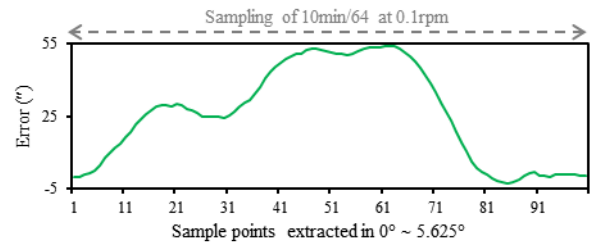


FIGURE 7. Short-period error of outer sense channel in primary test.

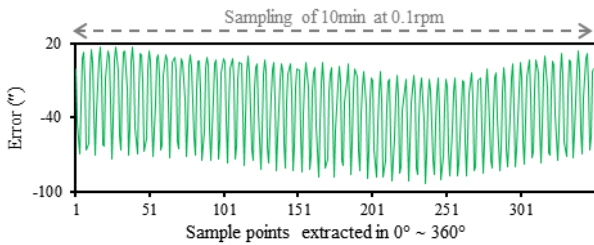


FIGURE 6. Full range error of inner sense channel in primary test.

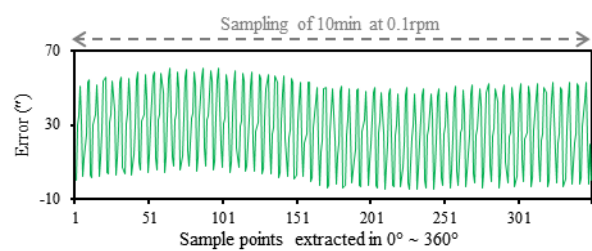


FIGURE 8. Full range error of outer sense channel in primary test.

two constants in the given prototype.

$$e_{\sin 1_1}(t, \theta) = k_1 \sin(N\theta) \cdot \cos(\omega t) + k_{11} \cos(\omega t) \quad (17)$$

$$e_{\cos 1_1}(t, \theta) = k_1 \cos(N\theta) \cdot \cos(\omega t) + k_{12} \cos(\omega t) \quad (18)$$

After the processing of the mixers, LPFs and amplifiers, signal (17) and (18) are transformed to two signals like (19) and (20) which contain one more part compared with

(9) and (10), i.e., DC parts k'_{11} and k'_{12} .

$$e'_{\sin 1_1}(t, \theta) = k'_1 \sin(N\theta) + k'_{11} \quad (19)$$

$$e'_{\cos 1_1}(t, \theta) = k'_1 \cos(N\theta) + k'_{12} \quad (20)$$

Assume that the DC parts k'_{11} and k'_{12} cause a measurement error δ_1 , then θ and δ_1 have the relation with signal (19) and

(20) as (21).

$$\tan(\theta + \delta_1) = \frac{k'_1 \sin(N\theta) + k'_{11}}{k'_1 \cos(N\theta) + k'_{12}} \quad (21)$$

It could be derived from (21):

$$\tan \delta_1 = \frac{\sqrt{k'^2_{11} + k'^2_{12}} \cdot \sin \left[\tan^{-1} \left(\frac{k'_{11}}{k'_{12}} \right) - N\theta \right]}{k'_1 + \sqrt{k'^2_{11} + k'^2_{12}} \cdot \sin \left[N\theta + \tan^{-1} \left(\frac{k'_{11}}{k'_{12}} \right) \right]} \quad (22)$$

Generally, k'_{11} and k'_{12} are far less than k'_1 , thus (22) can be simplified as (23).

$$\tan \delta_1 \approx \frac{\sqrt{k'^2_{11} + k'^2_{12}} \cdot \sin \left[\tan^{-1} \left(\frac{k'_{11}}{k'_{12}} \right) - N\theta \right]}{k'_1} \quad (23)$$

The value of δ_1 is very small in normal circumstances, as a result, we can get δ_1 using $\delta_1 \approx \tan \delta_1$. Equation (21) indicates that δ_1 varies N times when θ varies from 0° to 360° . It could be concluded that the EMF irrelevant with the rotor's rotation causes the first-order components of the short-period errors.

C. FIRST-ORDER ERROR SUPPRESSION

According to (19) to (21), we can know that reducing the influence of the DC parts k'_{11} and k'_{12} in the arctangent operation may be a way to reduce the above mentioned first-order components. In order to get DC parts k'_{11} and k'_{12} , the rotor was removed in the power on state of the prototype, and then the read data from ADC-1 and ADC-2 are saved as k'_{11} and k'_{12} . When the prototype came to normal work state, the read data from ADC-1 and ADC-2 subtract k'_{11} and k'_{12} before implementing arctangent operation in the angle computation.

After the conduction of the above error suppression method, the peak-peak value (maximum - minimum) of short-period error of inner sense channel decreased by about 55%, and that of outer sense channel decreased by about 45%. Fig. 9 to 12 show the error curves in the second test. Inner sense channel has the errors of

- 24.5''~14.7'' in the range of $0^\circ \sim 5.7^\circ$,
- 49.4''~20.8'' in the range of $0^\circ \sim 360^\circ$, while outer sense channel has the errors of
- 13.9''~17'' in the range of $0^\circ \sim 5.625^\circ$,
- 10.3''~30.3'' in the range of $0^\circ \sim 360^\circ$.

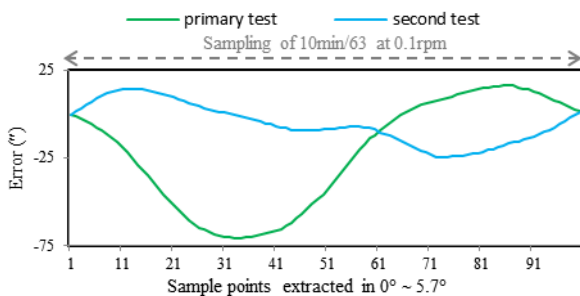


FIGURE 9. Short-period error of inner sense channel after first-order error suppression (second test).

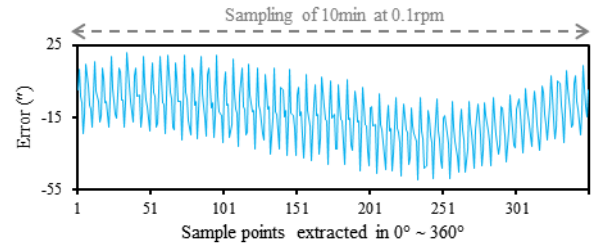


FIGURE 10. Full range error of inner sense channel after first-order error suppression.

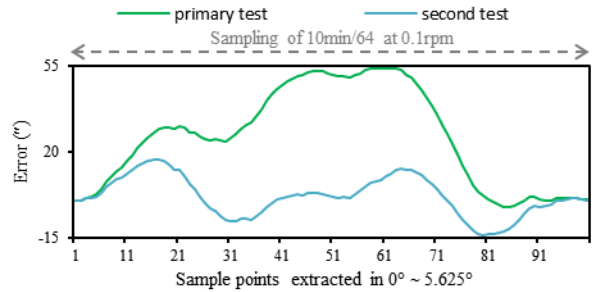


FIGURE 11. Short-period error of outer sense channel after first-order error suppression.

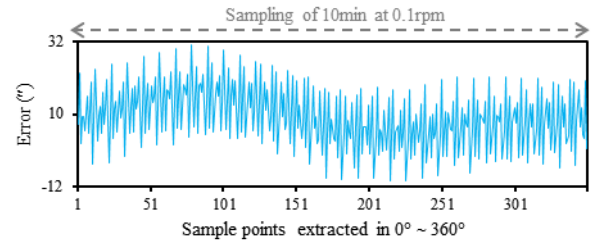


FIGURE 12. Full range error of outer sense channel after first-order error suppression.

Different from primary test, inner sense channel still has a significant first-order component in its short-period error, but outer sense channel has a significant second-order component in its short-period error.

D. ANALYSIS OF SECOND-ORDER ERROR

According to (9) to (12), the two outputs of every sense channel should be quadrature sine signals with same amplitude before inputting into the FPGA for the arctangent operation. However, if the signals for arctangent operation have quadrature or amplitude problems, there will be some errors introduced in the angle measurement. We also take the inner sense channel for example to analyze the influence of those two problems.

Assume that the quadrature problem causes signal (9) and (10) to be with the form as (24) and (25), and there is an error δ_{2_1} introduced in the angle computation, then θ and δ_{2_1} have the relation with signal (24) and (25) as (26).

$$e'_{\sin 1_21}(t, \theta) = k'_1 \sin(N\theta \pm \varphi) \quad (24)$$

$$e'_{\cos 1_21}(t, \theta) = k'_1 \cos(N\theta) \quad (25)$$

$$\tan(\theta + \delta_{2_1}) = \frac{k'_1 \sin(N\theta \pm \varphi)}{k'_1 \cos(N\theta)} \quad (26)$$

It could be derived from (26):

$$\begin{aligned} \tan \delta_{2_1} &= \frac{\pm 2 \sin \frac{\varphi}{2} \left[\cos^2(N\theta \pm \frac{\varphi}{4}) \cos^2 \frac{\varphi}{4} - \sin^2(N\theta \pm \frac{\varphi}{4}) \sin^2 \frac{\varphi}{4} \right]}{\cos^2(N\theta) + \sin(N\theta) \sin(N\theta \pm \varphi)} \end{aligned} \quad (27)$$

The value of φ is very small in most cases, thus $\sin^2(N\theta \pm \varphi/4) \sin 2(\varphi/4) \approx 0$, $\cos^2(N\theta) + \sin(N\theta) \cdot \sin(N\theta \pm \varphi) \approx 1$, (27) can be simplified as (28).

$$\tan \delta_{2_1} \approx \sin \frac{\varphi}{2} \cos^2 \frac{\varphi}{4} \left[\cos(2N\theta \pm \frac{\varphi}{2}) + 1 \right] \quad (28)$$

Assume that the amplitude problem causes signal (9) and (10) to be with the form as (29) and (30), and there is an error δ_{2_2} introduced in the angle computation, then θ and δ_{2_2} have the relation with signal (29) and (30) as (31).

$$e'_{\sin 1_22}(t, \theta) = k'_1 \sin(N\theta) \pm \Delta k'_1 \sin(N\theta) \quad (29)$$

$$e'_{\cos 1_22}(t, \theta) = k'_1 \cos(N\theta) \quad (30)$$

$$\tan(\theta + \delta_{2_2}) = \frac{k'_1 \sin(N\theta) \pm \Delta k'_1 \sin(N\theta)}{k'_1 \cos(N\theta)} \quad (31)$$

It could be derived from (31):

$$\tan \delta_{2_2} = \frac{\pm \frac{\Delta k'_1}{2} \sin(2N\theta)}{k'_1 \pm \frac{\Delta k'_1}{2} \sin^2(N\theta)} \quad (32)$$

Generally, $\Delta k'_1$ is also far less than k'_1 , thus (32) can be simplified as (33).

$$\tan \delta_{2_2} \approx \frac{\pm \Delta k'_1 \sin(2N\theta)}{2k'_1} \quad (33)$$

The values of δ_{2_1} and δ_{2_2} are also very small in normal circumstances, so we can get δ_{2_1} and δ_{2_2} using $\delta_{2_1} \approx \tan \delta_{2_1}$, $\delta_{2_2} \approx \tan \delta_{2_2}$. Equation (28) and (33) indicate that δ_{2_1} and δ_{2_2} vary $2N$ times when θ varies from 0° to 360° . It could be concluded that both quadrature and amplitude problems of the signals for arctangent operation will cause the second-order components of the short-period errors.

E. SECOND-ORDER ERROR SUPPRESSION

In the signal processing scheme as shown in Fig. 2 of the prototype, it is difficult to deal with the above described quadrature problem. However, the influence of the amplitude problem can be reduced easily by tuning the magnification of the amplifiers or tuning k'_1 and k'_2 in the FPGA software. The final absolute angle measurement of the prototype is defined by outer sense channel; therefore we further reduced short-period error of outer sense channel by overcoming the amplitude problem.

In order to tune k'_2 , the amplitudes of signal (11) and (12) were obtained first from the read data from ADC-1 and ADC-2 by rotating more than 5.625° . When the prototype

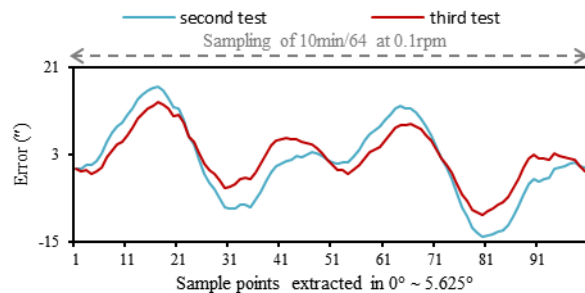


FIGURE 13. Short-period error of outer sense channel after second-order error suppression (third test).

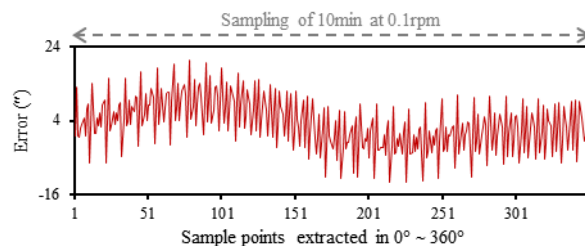


FIGURE 14. Full range error of outer sense channel after second-order error suppression.

came to normal work state, the amplitudes of signal (29) and (30) were tuned same by multiplying the smaller amplitude with a coefficient.

After the conduction of the amplitude tuning method, the peak-peak value of the short-period error of outer sense channel decreased by about 24%. Fig. 13 and 14 show the error curves in the third test. Outer sense channel has the errors of $-8.8'' \sim 14.7''$ in the range of $0^\circ \sim 5.625^\circ$, $-11.7'' \sim 20.6''$ in the range of $0^\circ \sim 360^\circ$.

V. SUMMARY

A planar absolute angle sensor based on eddy current effect is presented in this paper. It consists of a stator with two sense channels of excitation and pickup coils, a rotor with two circles of copper pieces. Every sense channel outputs two signals whose amplitudes vary with the rotor's rotation. Two sense channels have different periods and work together to realize absolute angle measurement. A sensor prototype has been developed using PCB technique. The prototype has 63 period inner sense channel and 64 period outer sense channel. Primary and second tests show the prototype has significant first- and second-order components in the short-period errors. In this paper, the causes of first- and second-order errors were analyzed, then the errors were compensated in a software way. Final test shows that the prototype has the measurement error of $-11.7'' \sim 20.6''$ in the range of $0^\circ \sim 360^\circ$. A summarized comparison in performance and manufacture of some other angular sensors with different measurement principles is shown in Table 1. The proposed inductive sensor employs a low cost measurement scheme and is very suitable for precision absolute angle measurement

TABLE 1. Comparison list of different angular sensors in performance and manufacture.

Sensor	Accuracy	Resolution	Cost	Easy to manufacture	Sensitive to environment
Optical based	High	High	High	Limited	Yes
Capacitive based	High	High	Moderate	Moderate	Yes
IncOder encoder	Low	Moderate	Low	Yes	No
Posic encoder	Low	Moderate	Low	Yes	No
RVDT	Low	Low	High	Limited	No
Resolver	Low	Low	High	Moderate	No
Inductosyn	High	Moderate	High	Limited	No
Sensor in [8]	Low	Moderate	Low	Yes	No
Sensor in [9]	Low	Low	Low	Yes	No
Sensor in [10]	Low	Low	Low	Yes	No
Sensor in this paper	Moderate	Moderate	Low	Yes	No

in harsh environments; thereby it is a good candidate of traditional sensors.

REFERENCES

- [1] (Aug. 1, 2021). *Absolute Rotary Encoders*. [Online]. Available: <https://netzerprecision.com>
- [2] D. Zheng, S. Zhang, S. Wang, C. Hu, and X. Zhao, "A capacitive rotary encoder based on quadrature modulation and demodulation," *IEEE Trans. Instrum. Meas.*, vol. 64, no. 1, pp. 143–153, Jan. 2015.
- [3] (Aug. 1, 2021). *Position Sensors*. [Online]. Available: <https://www.celeramotion.com/zettlex>
- [4] B. Aschenbrenner and B. G. Zagar, "Analysis and validation of a planar high-frequency contactless absolute inductive position sensor," *IEEE Trans. Instrum. Meas.*, vol. 64, no. 3, pp. 768–775, Mar. 2015.
- [5] B. Aschenbrenner and B. G. Zagar, "Planar high-frequency contactless inductive position sensor," in *Proc. IEEE Int. Instrum. Meas. Technol. Conf. (IMTC)*, May 2013, pp. 614–619.
- [6] (Aug. 1, 2021). *Rotary Inductive Encoders*. [Online]. Available: <https://www.posic.com>
- [7] Z. Zhang, F. Ni, Y. Dong, M. Jin, and H. Liu, "A novel absolute angular position sensor based on electromagnetism," *Sens. Actuators A, Phys.*, vol. 194, pp. 196–203, May 2013.
- [8] Q. Tang, D. Peng, L. Wu, and X. Chen, "An inductive angular displacement sensor based on planar coil and contrate rotor," *IEEE Sensors J.*, vol. 15, no. 7, pp. 3947–3954, Jul. 2015.
- [9] L. Ye, M. Yang, L. Xu, C. Guo, L. Li, and D. Wang, "Optimization of inductive angle sensor using response surface methodology and finite element method," *Measurement*, vol. 48, pp. 252–262, Feb. 2014.
- [10] B. P. Reddy, A. Murali, and G. Shaga, "Low cost planar coil structure for inductive sensors to measure absolute angular position," in *Proc. 2nd Int. Conf. Frontiers Sensors Technol. (ICFST)*, Shenzhen, China, Apr. 2017, pp. 14–18.
- [11] A. Babu and B. George, "Design and development of a new non-contact inductive displacement sensor," *IEEE Sensors J.*, vol. 18, no. 3, pp. 976–984, Feb. 2018.
- [12] K. R. Sandra, A. S. A. Kumar, B. George, and V. J. Kumar, "A linear differential inductive displacement sensor with dual planar coils," *IEEE Sensors J.*, vol. 19, no. 2, pp. 457–464, Jan. 2019.
- [13] N. Anandan and B. George, "Design and development of a planar linear variable differential transformer for displacement sensing," *IEEE Sensors J.*, vol. 17, no. 16, pp. 5298–5305, Aug. 2017.
- [14] A. Z. An, H. Z. Hui, Y. M. Yehan, and D. L. Da, "Analysis calculation and testing of rotary inductosyn angle measuring errors," in *Proc. 33rd Chin. Control Conf.*, Nanjing, China, Jul. 2014, pp. 8091–8096.
- [15] D. Chunyang and Y. Guijie, "Error analysis and compensation for inductosyn-based position measuring system," in *Proc. 38th IAS Annu. Meeting Conf. Rec. Ind. Appl. Conf.*, Salt Lake City, UT, USA, vol. 1, 2003, pp. 6–10.
- [16] S. Sarma and A. Venkateswaralu, "Systematic error cancellations and fault detection of resolver angular sensors using a DSP based system," *Mechatronics*, vol. 19, no. 8, pp. 1303–1312, Dec. 2009.
- [17] K. Kim, "Analysis on the characteristics of variable reluctance resolver considering uneven magnetic fields," *IEEE Trans. Magn.*, vol. 49, no. 7, pp. 3858–3861, Jul. 2013.
- [18] J. Figueiredo, "Resolver models for manufacturing," *IEEE Trans. Ind. Electron.*, vol. 58, no. 8, pp. 3693–3700, Aug. 2011.
- [19] S.-H. Hwang, H.-J. Kim, J.-M. Kim, L. Liu, and H. Li, "Compensation of amplitude imbalance and imperfect quadrature in resolver signals for PMSM drives," *IEEE Trans. Ind. Appl.*, vol. 47, no. 1, pp. 134–143, Jan./Feb. 2011.
- [20] S. Tumanski, "Induction coil sensors—A review," *Meas. Sci. Technol.*, vol. 18, no. 1, R31, Jan. 2007.
- [21] P. Luo, Q. Tang, H. Jing, and X. Chen, "Design and development of a self-calibration-based inductive absolute angular position sensor," *IEEE Sensors J.*, vol. 19, no. 14, pp. 5446–5453, Jul. 2019.
- [22] P. Luo, Q. Tang, and H. Jing, "Optimal design of angular displacement sensor with shared magnetic field based on the magnetic equivalent loop method," *Sensors*, vol. 19, no. 9, p. 2207, May 2019.



placement measurement technology.

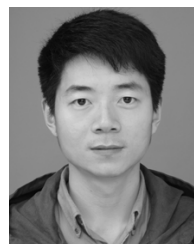
WENZHENG GAO received the B.Eng. degree in computer and automatic control from Sichuan University, Chengdu, China, in 1988, and the M.Eng. degree in communication and electronic engineering from the Nanjing University of Aeronautics and Astronautics, Nanjing, China, in 2007.

Since 1988, he has been working with the Department of Control Equipment, Lianyungang JARI Electronics Company Ltd., Lianyungang, Jiangsu. His research interests include angular displacement measurement technology and computer and automatic control technology.



HONG SHI received the B.Eng. degree in electrical engineering and automation from the Harbin Institute of Technology, Harbin, China, in 2012.

Since 2012, he has been working with the Department of Control Equipment, Lianyungang JARI Electronics Company Ltd., Lianyungang, Jiangsu. His research interests include angular displacement measurement technology and computer and automatic control technology.



QIFU TANG (Member, IEEE) received the M.Eng. degree in measurement and instrumentation from the Chongqing University of Technology (CQUT), Chongqing, China, in 2012, and the Ph.D. degree in mechanical design and theory (engineering) from Chongqing University, Chongqing, in 2015.

Since 2016, he has been working with the Engineering Research Center of Mechanical Testing Technology and Equipment, Ministry of Education, CQUT. His research interests include measurement technologies and instruments of displacement.

...